Journal of Power Sources 217 (2012) 381–391

Contents lists available at SciVerse ScienceDirect

Journal of Power Sources

journal homepage: www.elsevier.com/locate/jpowsour

Water transport and flooding in DMFC: Experimental and modeling analyses

M. Zago [a,*], A. Casalegno [a], C. Santoro [b], R. Marchesi [a]

[a] Politecnico di Milano, Department of Energy, Via Lambruschini 4, 20156 Milano, Italy
[b] University of Connecticut, Department of Civil and Environmental Engineering, 06269 Storrs, CT, United States

HIGHLIGHTS

- We analyzed experimentally water transport and flooding in DMFC.
- We proposed and validated a model of water transport and flooding in DMFC.
- Water flow through cathode diffusion layer is due to vapor diffusion and liquid permeation.
- Flooding implies both superficial and bulk pores obstruction of diffusion layer.
- We developed correlations to simulate flooding effects.

ARTICLE INFO

Article history:
Received 12 March 2012
Received in revised form
1 June 2012
Accepted 5 June 2012
Available online 13 June 2012

Keywords:
Direct methanol fuel cell
Water transport
Flooding
Model

ABSTRACT

Water transport control is the major issue of direct methanol fuel cell. High water flow rates through the fuel cell imply extra water feeding at the anode and flooding at the cathode. In the present work, water transport and flooding in the direct methanol fuel cell are investigated through both experimental and modeling analyses and an interpretation of such phenomena is proposed. The model is validated on the experimental data of two different fuel cells in an extensive range of operating conditions. The analysis elucidates that water transport through the cathode diffusion layer is determined by vapor diffusion, slightly affected by current density, and by liquid water permeation proportional to current density, that occurs when liquid pressure in the electrode exceeds a threshold value. To simulate the effects of cathode diffusion layer flooding two mechanisms must be considered simultaneously: superficial pore obstruction, proportional to liquid water concentration in cathode channel, and bulk pore obstruction, proportional to liquid water permeation. The modeling analysis proposes the correlations to reproduce the effects of cathode flooding and permits to discuss the onset and magnitude of such phenomenon and the influence of micro-porous layer.

1. Introduction

The direct methanol fuel cell (DMFC) receives considerable attention as a leading candidate power source for portable and automotive applications. The widely use of the DMFC technology is still hindered by some technological issues, among which the water management is one of the most important [1–4]. DMFCs are fed with a liquid mixture composed by water and methanol and the water as well as the methanol flow through the membrane from the anode to the cathode [5,6]. Water crossover through the membrane may cause two problems named anodic water consumption [7–9] and cathode flooding [10–17]. The increased water consumption, caused by water crossover through the membrane, implies the necessity of additional water feeding and storage, reducing the compactness of the DMFC systems [10,11]. Secondly, the high rate of water crossover increases the cathode flooding, especially during dynamic operation, therefore a suitable management of water transport and flooding is considerably important in order to improve DMFC performance and lifetime.

The present work aims to increase the understanding of water transport and flooding in DMFC, proposing a model able to describe and reproduce experimental data and an exhaustive interpretation of such phenomena.

During the last years, water crossover in DMFCs has been extensively studied [10–24]. It has been found that the cathode gas diffusion layer (GDL), composed by a carbon macro-porous layer and usually by an additional micro-porous layer (MPL) coated on it, plays an important role in both water crossover through the membrane and water removal to the cathode. The effect of cathode GDL properties on water transport in DMFCs has been widely investigated [10–17,22–25]. Several works studied also how to minimize water transport, especially in passive DMFC, modifying the GDLs characteristics in anode and cathode [17,26–28]. The characterization of flooding onset and its effect on the performance has not been significantly examined, despite this phenomenon

* Corresponding author. Tel.: +39 02 2399 3874; fax: +39 02 2399 3913.
E-mail address: matteo.zago@mail.polimi.it (M. Zago).

0378-7753/$ – see front matter © 2012 Elsevier B.V. All rights reserved.
http://dx.doi.org/10.1016/j.jpowsour.2012.06.022

could occur also in optimized DMFC during dynamic operation or after GDL degradation [29]. Modeling analyses dealt with water transport in DMFC [30–40]. Schultz and Sundmacher [33] presented a one-dimensional dynamic model, validated also on water transport experimental measurements, neglecting the two-phase behavior in both diffusion layers and flooding effects. Ko et al. [34] developed a 1-D model where the two-phase behavior was considered, but water diffusion in gas phase through the cathode GDL was neglected and the model was validated on a single operating condition. Yang and Zhao [35,36] presented a complete two-dimensional and two-phase DMFC model, validated only on the experimental performance and a limited set of operating conditions was considered. In previous works [37–39], Casalegno et al. presented a 1-D model validated with respect to overall polarization, anode polarization, methanol cross-over, showing a good agreement with the experimental data, but water transport was not analyzed in detail. Pasaogullari and Wang [40] developed a two-phase numerical model to analyze the multi-layer GDL in PEMFCs. They particularly investigated the effects of porosity, thickness and hydrophobicity of an MPL on the two-phase transport [40]. The results showed that the addition of the MPL between catalyst layer and GDL could enhance liquid water removal and reduce the liquid saturation in the catalyst layer.

In the literature, the mechanisms that regulate water transport in DMFC are not fully consolidated and limited effort has been dedicated to analyze flooding onset and its consequences on DMFC operation. A detailed comprehension of such phenomena is required to further optimize components and operation strategies.

This work aims to propose a combined experimental and modeling analysis in order to increase the understanding of the mechanisms that regulate water transport and flooding in DMFC through the following steps:

- a model of water transport and cathode flooding is proposed analyzing experimental data obtained with different operating conditions and cathode GDL features;
- the previously developed DMFC model [37–39] is integrated, in order to validate the proposed interpretation in an extensive range of operating conditions, using three different sets of measure: polarization curves, methanol crossover and water flow-rate at cathode outlet;
- correlations able to reproduce the effect of cathode GDL flooding are proposed as a tool for further studies and components optimization.

2. Experimental setup

The experimental analyses of DMFC performance and methanol crossover are carried out implementing, in the equipment previously developed [41], the measure of water concentration at cathode outlet.

Cathode side was modified introducing, Fig. 1:

- a heat exchanger to warm up the cathode exhaust to evaporate eventual liquid water;
- a thermo-hygrometer for humidity (uncertainty 2%) and temperature (uncertainty 0.2 °C) measurements, located in a thermo-stated housing to avoid condensation.

The above modifications permit to measure the water content in the cathode exhaust $X^{c}_{H_2O}$ and considering the mass balance equations (1)–(8) reported in Ref. [41], the water flow at the cathode outlet is given by:

$$N^{H_2O,c}_{out} = X^{c}_{H_2O} \cdot N^{c}_{out,tot} \quad (1)$$

These new components have negligible pressure drop and do not increase considerably the transient time necessary to reach steady state in the vessels.

The experimental analysis is carried out on two of the three MEAs already characterized in Ref. [41]: MEA GG, GDL without MPL

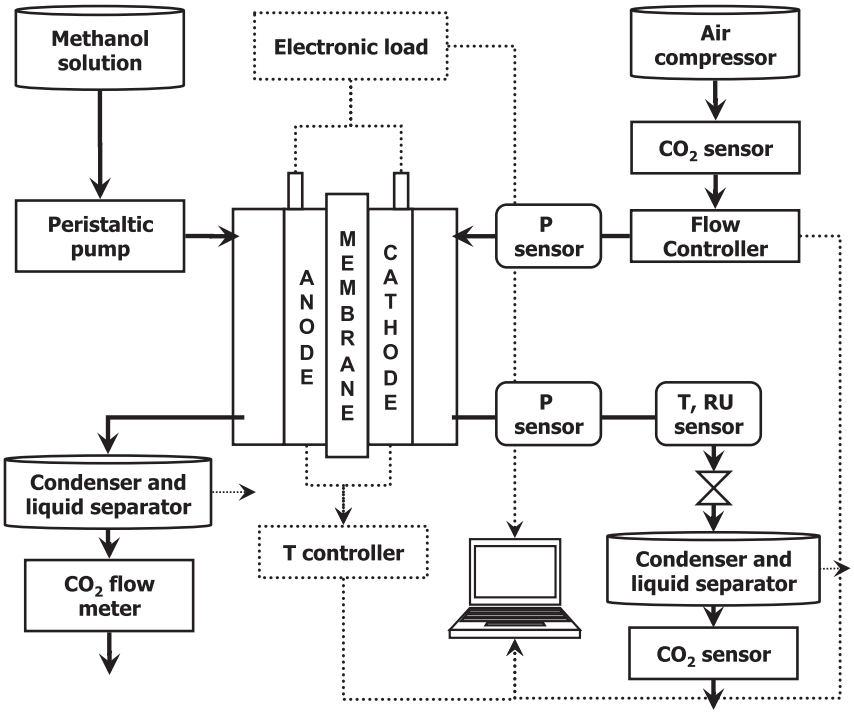

Fig. 1. Experimental setup scheme.

Table 1
Investigated operating conditions.

MEA	T [K]	X_{CH_3OH} [wt%]	m_{air} [g min^{-1}]	p^c_{in} [kPa]	p^c_{out} [kPa]
GM	333	3.25	0.62	112	108
GM	333	3.25	0.62	151	147
GM	333	3.25	1.14	122	115
GM	333	3.25	1.14	155	148
GM	333	6.5	0.62	112	108
GM	333	6.5	0.62	151	147
GM	333	6.5	1.14	122	115
GM	333	6.5	1.14	155	148
GM	353	3.25	0.62	112	108
GM	353	3.25	1.14	122	115
GM	353	6.5	0.62	112	108
GM	353	6.5	1.14	122	115
GG	333	3.25	0.62	112	108
GG	333	3.25	1.14	122	115
GG	333	6.5	0.62	112	108
GG	333	6.5	1.14	122	115
GG	333	6.5	1.14	155	148
GG	353	6.5	1.14	122	115

on both anode and cathode; MEA GM, GDL without MPL at anode and GDL with MPL at cathode.

A set of the measurement already examined in Ref. [41] have been reproduced by means of the improved experimental setup. Note that in all the investigated operating conditions (Table 1[1]) the anode flow rate is set at 1 g min^{-1} and the anode mean pressure at 105 kPa. The results of performance and methanol crossover reported in Ref. [41], as well as measurement uncertainty and reproducibility evaluation, remain valid. The uncertainty associated to the measurement of water flow is evaluated, according to Ref. [42], equal to 7% in the whole investigated range.

3. Experimental analyses

3.1. Influence of operating conditions

In Fig. 2 the water flow at cathode outlet, in function of current density, is reported for different operating conditions. A general behavior can be distinguished: at low current density the water flow is approximately constant, a sort of plateau is evident, then it increases, in some cases suddenly, with an approximately linear trend. This behavior suggests the presence of two different mechanisms regulating water transport to cathode channel. A possible interpretation could be based on the two main mechanisms of water transport through GDL reported in literature: diffusion in vapor phase and permeation in liquid phase. The plateau could be caused by water vapor diffusion through the cathode GDL, determined by an approximately constant water concentration along the cathode electrode. Small current density variations do not affect significantly water concentration profile. Instead at higher current density the linear trend could be due to the onset of liquid water permeation, forced by enhanced electro-osmotic drag and water production at cathode, both directly proportional to current density.

This preliminary interpretation is discussed analyzing the experimental results in different operating conditions.

The proposed plateau origin is coherent with the following considerations regarding Fig. 2a:

- an increase of airflow rate induces a decrease of water concentration in cathode channel, as a consequence the water concentration difference across the GDL and the relative diffusive flow grow; therefore the water flow at cathode outlet, i.e. the plateau value, increases;
- an increase of temperature determines a general increment of both GDL diffusivity and water concentration at cathode electrode, related to saturation concentration; thus the water flow at cathode outlet increases;
- at higher cathode mean pressure, the total gas mixture concentration increases, therefore at similar water concentration, water fraction $X^c_{H_2O}$ lowers; consequently the plateau value decreases, according to equation (1).

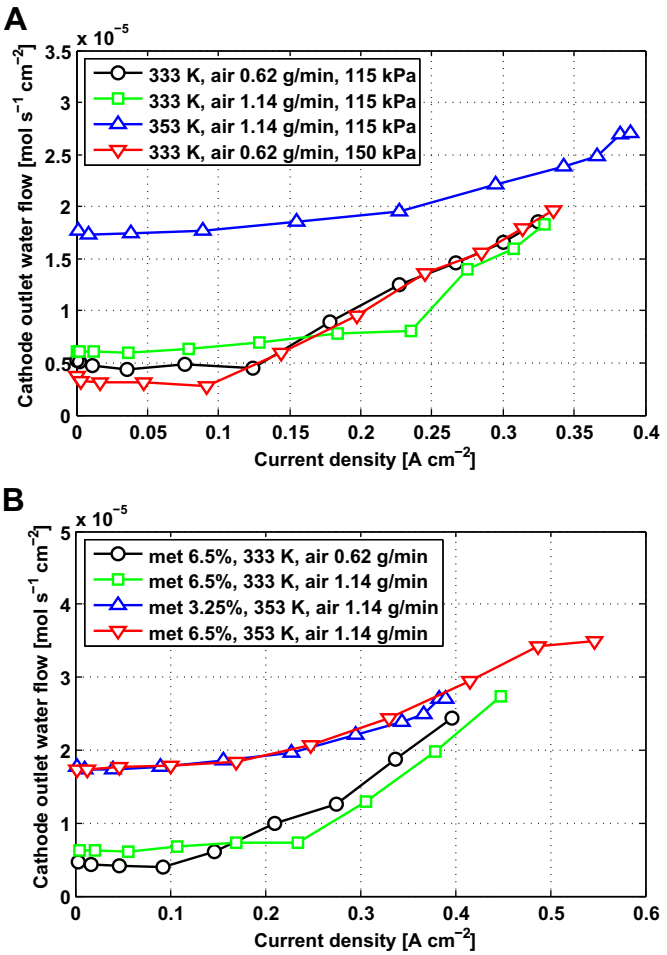

Fig. 2. Influence of operating conditions on water flux (MEA GM): a) methanol concentration 3.25%; b) cathode pressure 1 bar.

Regarding the linear behavior at higher current density, the curves at lower temperature assume the same linear trend, coherently with the proposed dependence on electro-osmotic drag and water production, not affected considerably by the airflow or pressure variation.

A further confirmation of the proposed interpretation is obtained comparing the experimental results at higher methanol concentration, Fig. 2b. Doubling methanol concentration, the plateau values do not change significantly, while the performances are considerably different, Fig. 3, as well as the methanol crossover [41]. Therefore, the plateau is confirmed to be influenced exclusively by cathode flow conditions. Moreover a linear trend with a similar slope is present, as expected in these operating conditions, Fig. 2b.

An additional evaluation of the proposed interpretation is reported in the modeling section.

[1] In the followings unpressurized cathode is named as 1 bar, instead pressurized cathode is named as 1.5 bar.

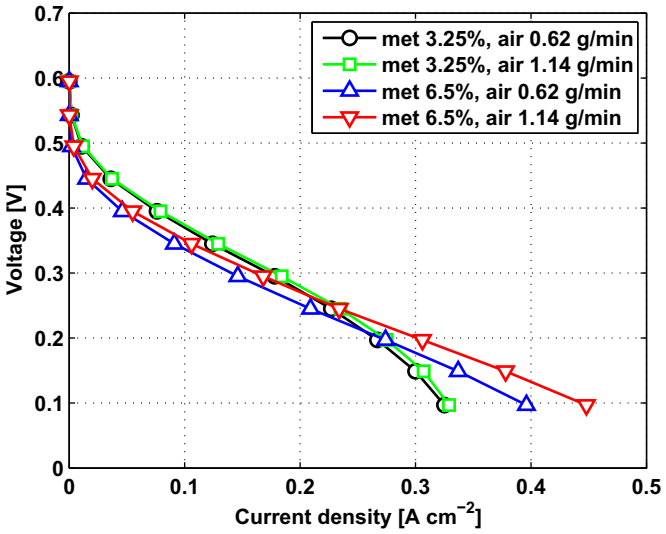

Fig. 3. Influence of operating conditions on performance at 333 K and 1 bar (MEA GM).

A consequence of the considerable water transport through the cathode GDL is the pore flooding that hinders oxygen transport and DMFC performance. Liquid water permeation through the GDL is expected to cause a significant pores obstruction. A comparison of polarization curves in different operating conditions is reported in Fig. 3. At low methanol concentration an increase of airflow rate determines negligible variations of DMFC performance. In contrast, water flow at cathode outlet varies significantly and considerable water permeation is expected to occur in both cases at high current density. This behavior can be explained considering that the performance at high current density is strongly limited by the anode feeding, worsen by low methanol concentration, as discussed previously in Ref. [41]. In such conditions, the effect of an oxygen transport hindered by flooding is undetectable.

The behavior is different at higher methanol concentration: the performance is not anymore limited by anode feeding but a negative effect of airflow reduction is evident. The water transport increases at high current density when the airflow decreases, Fig. 2b. Both the lower airflow rate and the increased water flow imply a reduction of oxygen concentration at cathode electrode leading to a decrease in the performance. The performance decrease could be due to such oxygen concentration reduction or to a further pore flooding effect, but it cannot be distinguished from these experimental results. A further interpretation of this aspect is discussed in the next section.

3.2. Cathode MPL influence

In order to clarify the effect of water transport on DMFC performance, the results regarding the MEA GG (without cathode MPL) and the MEA GM (with cathode MPL) are discussed and compared. In Fig. 4a, the water flow at the cathode outlet for the two MEAs is reported. An enhanced water transport is evident in the MEA without MPL: the mass transfer resistance at cathode side decreases eliminating the additional micro-porous layer, coherently with the results reported in Ref. [43]. The plateau rises approximately by a factor 1.5 in both the two temperature conditions. Moreover it is confirmed that the enhanced methanol crossover is due to the increment of water transport that causes an increase of the average methanol concentration at anode side, as suggested in Ref. [41].

A general improvement of performance is evident with cathode without MPL, Fig. 4b, accordingly to the enhanced mass transport through the GDL that increases oxygen concentration at cathode

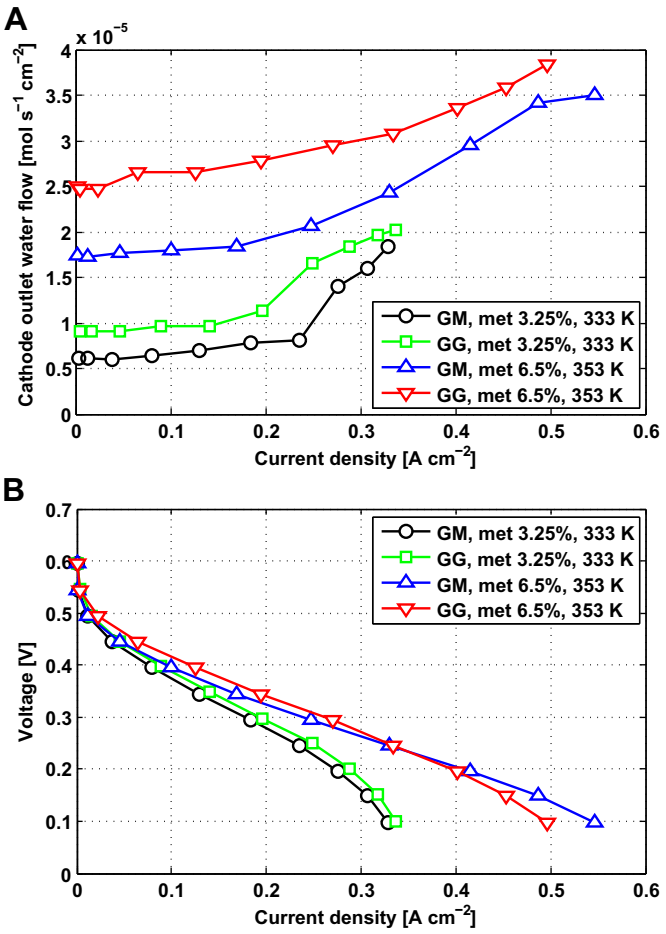

Fig. 4. Influence of operating conditions on a) water flux and b) performance with airflow of 1.14 g min^{-1} at 1 bar.

electrode. A clear exception is evident: the performance of MEA GG drops and becomes lower than MEA GM one at current density higher than 0.35 A cm^{-2}. This behavior has been already found in literature [44–46] and it is probably caused by a considerable GDL flooding phenomenon.

In order to confirm flooding presence and quantify its effect a specific modeling analysis is reported in the followings.

4. Modeling

In this work the model already presented in Refs. [37,38] is integrated with equations, that describe water transport phenomena and flooding effects. The original model includes the complete mass balance, considering two-phase anode flow, but single-phase cathode flow and consequently cathode flooding was not considered. Moreover the water crossover is calculated as the sum of electro-osmosis and liquid phase diffusion, neglecting liquid water concentration at cathode side.

In the new model the implementation of water transport phenomena, including two-phase cathode flow and flooding, is introduced to validate the proposed interpretations and elucidate flooding effects on performance.

4.1. Water transport description

According to the proposed interpretation, the water fluxes through a DMFC are those illustrated in Fig. 5. The water availability at anode side is considered to be very high and the anode GDL is

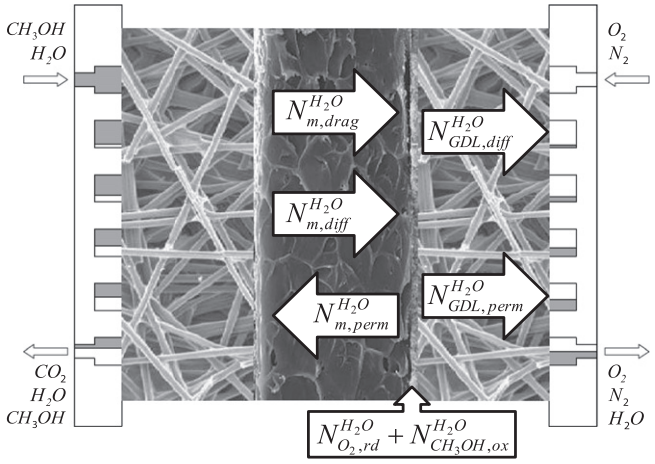

Fig. 5. Water fluxes through the DMFC.

assumed to be flooded with fully liquid pathways [17], therefore the water transport through the MEA is generally regulated by water transport through membrane and cathode diffusion layer, in agreement with the literature [44].

4.1.1. Membrane

The water cross-over through the membrane is due to three transport mechanisms [14,47,48], electro-osmotic drag by proton transport, diffusion by water concentration gradient and convection by hydraulic pressure gradient, as reported in the following equation:

$$N^{H_2O}_{m,cross} = N^{H_2O}_{m,drag} + N^{H_2O}_{m,diff} - N^{H_2O}_{m,perm} \quad (2)$$

The water flux due to electro-osmotic drag can be determined from:

$$N^{H_2O}_{m,drag} = \eta_d \cdot \frac{i}{F} \quad (3)$$

Permeation flux depends on the liquid pressure difference across the membrane and can be expressed as:

$$N^{H_2O}_{m,perm} = \frac{K_m \cdot \rho_{H_2O}}{\mu_{H_2O} \cdot M_{H_2O} \cdot l_m} \cdot \left(p^{c,L}_{H_2O} - p^{a,L}_{H_2O}\right) \quad (4)$$

Since the flow velocity through the liquid pathways of anode GDL can be neglected, $p^{a,L}_{H_2O}$ is assumed equal to the total pressure in the anode flow channel p^a. At cathode side material hydrophobicity and water transport could determine a considerable capillary pressure, thus $p^{c,L}_{H_2O}$ can be significantly greater than gas pressure. The capillary pressure is proportional to water saturation in the electrode [49] and consequently to liquid concentration at membrane interface [27]:

$$\Delta p_c = p^{c,L}_{H_2O} - p^{c,G}_{H_2O} \propto s \propto C^{m,c,L}_{H_2O} \quad (5)$$

This dependence is uncertain and strongly affected by material characteristics, in fact a general correlation is not available in literature.[2] In the present work a first order dependence is assumed:

$$C^{m,c,L}_{H_2O} = W_2 \cdot \left(p^{c,L}_{H_2O} - p^{c,G}_{H_2O}\right) \quad (6)$$

where W_2 is calibrated over experimental data.

Due to negligible gas pressure gradient across the entire porous media, $p^{c,g}_{H_2O}$ can be assumed equal to total cathode pressure p^c, as widely accepted in literature [40]. Generally, under typical operating conditions $p^{c,L}_{H_2O}$ is greater than $p^{a,L}_{H_2O}$, leading to a permeation flux from cathode to anode. Both anode and cathode total pressures are assumed to vary linearly with channel length x:

$$p^{a,c}_{in} - \left(p^{a,c}_{in} - p^{a,c}_{out}\right) \cdot \frac{x}{L} = p^{a,c} \quad (7)$$

The flux of water due to liquid diffusion can be expressed as:

$$N^{H_2O}_{m,diff} = \frac{D_{m,H_2O}}{l_m} \cdot \left(C^{m,a,L}_{H_2O} - C^{m,c,L}_{H_2O}\right) \quad (8)$$

where $C^{m,a,L}_{H_2O}$ and $C^{m,c,L}_{H_2O}$ represent, respectively, liquid water concentrations at the membrane interfaces. Generally, the magnitude of both $C^{m,a,L}_{H_2O}$ and $C^{m,c,L}_{H_2O}$ depends on the properties of the MEA and the operating conditions. Moreover in literature magnitude and direction of water diffusion flux are controversial [50,51]. In this work $C^{m,a,L}_{H_2O}$ is assumed equal to the liquid concentration corresponding to a fully hydrated membrane, with water content about 30 [52]; $C^{c,L}_{H_2O}$ is already defined in equation (6).

Equation (2) substitutes equation (27) of the original model [37]. The variable $P^{c,L}_{H_2O}$ is determined considering the water transport through gas diffusion layer.

4.1.2. Cathode diffusion layer

The water flow through cathode GDL, $N^{H_2O}_{GDL}$, is equal to the sum of water cross-over through the membrane, $N^{H_2O}_{m,cross}$, and water sources in the cathode catalyst layer due to methanol cross-over oxidation, $N^{H_2O}_{CH_3OH,ox}$, and to oxygen reduction, $N^{H_2O}_{O2,rd}$, according to:

$$N^{H_2O}_{GDL} = N^{H_2O}_{CH_3OH,ox} + N^{H_2O}_{O_2,rd} + N^{H_2O}_{m,cross} \quad (9)$$

$$N^{H_2O}_{GDL} = 2 \cdot N^{H_2O}_{CH_3OH,cross} + \frac{i}{2 \cdot F} + N^{H_2O}_{m,cross} \quad (10)$$

As reported in Ref. [53], the water flow through GDL is due to different contributions: diffusion and permeation in gas phase and permeation in liquid phase. The assumption of a constant gas-phase pressure across the entire porous media [40] allows neglecting gas permeation through the GDL. Therefore water transport through cathode GDL occurs mainly by vapor diffusion, $N^{H_2O}_{GDL,diff}$, and liquid permeation, $N^{H_2O}_{GDL,perm}$, according to the proposed interpretation.

The two-phase behavior at cathode side is simplified as a plug flow, where plugs and bubbles have the same local velocity. Equation (14) of the original model [37] is replaced by the following:

$$\frac{h^c}{2} \cdot \frac{\partial\left(v^c \cdot \overline{C}^c_{H_2O}\right)}{\partial x} = N^{H_2O}_{GDL} = N^{H_2O}_{GDL,diff} + N^{H_2O}_{GDL,perm} \quad (11)$$

$\overline{C}^c_{H_2O}$ is the time-averaged total water concentration in the cathode channel, defined as:

$$\begin{cases} \overline{C}^c_{H_2O} = C^{c,G}_{H_2O}, \text{ if } \overline{C}^c_{H_2O} \le C^{sat}_{H_2O} \\ \overline{C}^c_{H_2O} = \varepsilon^c \cdot C^{sat}_{H_2O} + (1-\varepsilon^c) \cdot \dfrac{\rho_{H_2O}}{M_{H_2O}}, \text{ if } \overline{C}^c_{H_2O} > C^{sat}_{H_2O} \end{cases} \quad (12)$$

where ε^c is the cathode volumetric gas fraction.

According to Ref. [43], the overall mass transport coefficient in gas-phase can be determined from:

$$R^G_{H_2O} = R^G_{H_2O,conv} + R^G_{H_2O,diff} = \frac{1}{h_{conv}} + \left(\frac{l_{GDL}}{D_{GDL}} + \frac{l_{MPL}}{D_{MPL}}\right) \quad (13)$$

[2] Note that the correlations reported in literature [27] are generally between the saturation and the dissolved water concentration in the ionomer of the catalyst layer, that is different from membrane one, $C^{m,c,L}_{H_2O}$.

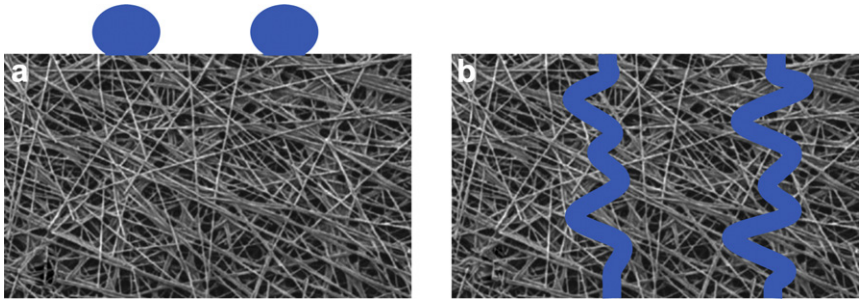

Fig. 6. a) Superficial pores obstruction. b) Bulk pores obstruction.

where h_{conv} is the convective mass transport coefficient in the channel. The resulting water flux can thus be expressed as:

$$N^{H_2O}_{GDL,diff} = \frac{\left(C^{t,G}_{H_2O} - C^{c,G}_{H_2O}\right)}{R^{G}_{H_2O}} \tag{14}$$

where $C^{t,G}_{H_2O}$, the water vapor concentration in the cathode electrode, depends on the liquid concentration in the membrane interface $C^{m,c,L}_{H_2O}$; the data reported in Ref. [54] are interpolated with a third order polynomial.

The interpretation of water permeation onset at high current density is reported in the experimental analysis discussion and it is implemented in the model as follows. Water diffusion through cathode GDL led to an increase of water concentration along the cathode channel: this transport mechanism becomes less and less considerable along cathode channel when its driving force diminishes.

This implies an increase of the liquid pressure in the cathode electrode, $p^{c,L}_{H_2O}$: when it becomes greater than a threshold value, p_{lim}, liquid permeation through cathode GDL occurs. The values of $p^{c,L}_{H_2O}$ and $N^{H_2O}_{GDL,perm}$ are calculated by solving the following water balance at electrode–GDL interface:

$$N^{H_2O}_{m,drag} + N^{H_2O}_{m,diff} - N^{H_2O}_{m,perm} + N^{H_2O}_{CH_3OH,ox} + N^{H_2O}_{O_2,rd} = N^{H_2O}_{GDL,diff} + N^{H_2O}_{GDL,perm} \tag{15}$$

considering the following two cases

$$\text{if } p^{c,L}_{H_2O} \le p_{lim} \begin{cases} N^{H_2O}_{m,perm} = \dfrac{K_m \cdot \rho_{H_2O}}{\mu_{H_2O} \cdot M_{H_2O} \cdot l_m} \cdot \left(p^{c,L}_{H_2O} - p^{a,L}_{H_2O}\right) \\ N^{H_2O}_{m,diff} = \dfrac{D_{m,H_2O}}{l_m} \cdot \left(C^{m,a,L}_{H_2O} - W_2 \cdot p^{c,L}_{H_2O}\right) \\ N^{H_2O}_{GDL,perm} = 0 \end{cases}$$

$$\text{if } p^{c,L}_{H_2O} > p_{lim} \begin{cases} N^{H_2O}_{m,perm} = \dfrac{K_m \cdot \rho_{H_2O}}{\mu_{H_2O} \cdot M_{H_2O} \cdot l_m} \cdot \left(p_{lim} - p^{a,L}_{H_2O}\right) \\ N^{H_2O}_{m,diff} = \dfrac{D_{m,H_2O}}{l_m} \cdot \left(C^{m,a,L}_{H_2O} - W_2 \cdot p_{lim}\right) \\ N^{H_2O}_{GDL,perm} = N^{H_2O}_{m,drag} + N^{H_2O}_{m,diff} - N^{H_2O}_{m,perm} + N^{H_2O}_{CH_3OH,ox} + N^{H_2O}_{O_2,rd} - N^{H_2O}_{GDL,diff} \end{cases} \tag{16}$$

4.2. Flooding description

It is widely known that flooding reduces fuel cell performance, while the effective mechanisms are not fully understood. Many authors agree on the main reason known as the hindrance of oxygen transport caused by GDL and electrode pore obstruction with liquid water [34,36,49]. The following model does not pretend to be a detailed and exhaustive description of such complex phenomenon, but a tool to increase its understanding and for further studies. In this work, flooding effects are modeled considering two contributions:

- superficial pores obstruction, Fig. 6a: if water concentration in cathode channel exceeds the saturation value, drops of water condense on GDL surface.[3] This effect is considered as a reduction of GDL diffusivity proportional to liquid water concentration [43], where correlations for similar GDLs are proposed. A suitable one is adapted as follows:

$$D^{c}_{GDL,O_2} = D^{c}_{GDL,eff,O_2} - B_1 \cdot \left(\overline{C}^{c}_{H_2O} - C^{sat}_{H_2O}\right)^{0.58} \tag{17}$$

  where B_1 is derived from the model calibration, Section 4.2;
- bulk pores obstruction, Fig. 6b: if liquid water permeation through cathode GDL occurs, the flow obstructs GDL pores, establishing liquid pathways [55]. Both effects imply a reduction of GDL diffusivity proportional to liquid water permeation through cathode GDL.[4] To take into account this effect a correlation is proposed:

$$D^{c}_{GDL,O_2} = D^{c}_{GDL,eff,O_2} - B_2 \cdot \left(N^{H_2O}_{GDL,perm}\right)^{B_3} \tag{18}$$

  where B_2 and B_3 are obtained by model calibration.

4.3. Model validation

The proposed DMFC model is constituted by 7 differential equations, 29 algebraic equations, 36 variables and two correlations to take into account flooding effects, equations (17) and (18). This DAE system is solved in MATLAB® environment, applying the appropriate initial conditions, regarding inlet flows, potential difference and fuel cell temperature and pressures. The values of the parameters utilized for the calculation are reported in Table 2.

The calibration procedure consists in the minimization of the residuals between model estimation and experimental results and permits to determine the values of the most uncertain physic-chemical parameters. The considered experimental data set for calibration concern the MEA GM and is composed of 132 measurement points, coming from 12 polarization curves, Table 1.

[3] Generally liquid water is not present in bulk GDL because of its high hydrophobicity.

[4] Bulk obstruction of MPL is neglected, because its saturation is generally much lower than GDL one [36]. Anyway the GDL diffusivity reduction includes also the eventual MPL one.

Table 2
Parameters utilized for the calculation.

$D^{c}_{GDL,eff}$	$1.59 \times 10^{-1} \times (T/333)^{1.75}$	$cm^2\ s^{-1}$	[43]
$D^{c}_{MPL,eff}$	W_3	$cm^2\ s^{-1}$	Calibrated
$D^{a,L}_{CH_3OH}$	$10^{-5.4163-999.778/T} \times 10^4$	$cm^2\ s^{-1}$	[64]
$D^{a,G}_{CH_3OH}$	I_1	$cm^2\ s^{-1}$	Calibrated
D_{m,CH_3OH}	$C_1 \times \exp(C_2 \times (1/303 - 1/T))$	$cm^2\ s^{-1}$	Calibrated
D_{m,H_2O}	$4.17 \times 10^{-4} \times 22 \times (161\exp(-22) + 1) \times \exp(-2436/T)$	$cm^2\ s^{-1}$	[27]
h_{conv} (@333 K)	0.115×10^2	$cm\ s^{-1}$	[43]
h_{conv} (@353 K)	0.125×10^2	$cm\ s^{-1}$	[43]
C^{a}_{ref}	1×10^{-3}	$mol\ cm^{-3}$	[56]
C^{c}_{ref}	7.25×10^{-6}	$mol\ cm^{-3}$	[56]
γ^a	I_2	–	Calibrated
γ^c	1	–	[30]
α^c	0.6	–	[38]
α^a	I_3	–	Calibrated
i^a	$I_4 \times \exp(I_5/R \times (1/353 - 1/T))$	$A\ cm^{-2}$	Calibrated
i^c	$1.37 \times 10^{-4} \times \exp(50{,}750/R \times (1/353 - 1/T))$	$A\ cm^{-2}$	[38]
σ_m	$0.073 \times \exp(1268 \times (1/298 - 1/T))$	$\Omega^{-1}\ cm^{-1}$	[57]
K_m	W_1	m^2	Calibrated
$p_{lim,MPL}$	6700	Pa	[55]
$C^{m,c,L}_{H_2O}$	$W_2 \times (p^{c,L}_{H_2O} - p^{c,G}_{H_2O})$	$mol\ cm^{-3}$	Calibrated
n_d	$W_4 \times \exp(1029 \times (1/333 - 1/T))$	–	Calibrated
n_{dx}	$C_3 \times \exp(C_4 \times (1/333 - 1/T))$	–	Calibrated
ρ_{H_2O}	$(-0.0028 \times (T-273)^2 - 0.1757 \times (T-273) + 1003.8) \times 10^{-3}$	$g\ cm^{-3}$	[64]
μ_{H_2O}	3.56×10^{-4}	Pa s	[64]
K_{H,CH_3OH}	$2.2 \times \exp(5200 \times (1/T - 1/298))$	$mol\ J^{-1}$	[64]
K_{H,CO_2}	$3.5 \times \exp(2400 \times (1/T - 1/298))$	$mol\ J^{-1}$	[64]
E_0	1.21	V	–
F	94,495	$C\ mol^{-1}$	–
R	8314	$J\ mol^{-1}\ K^{-1}$	–
l_m	0.018	cm	–
l^c_{MPL}	0.005	cm	–
l^c_{GDL}	0.025	cm	–
l^a_{GDL}	0.03	cm	–
A_{cell}	22.1	cm^2	–
h^a	0.08	cm	–
h^c	0.08	cm	–
L	138.125	cm	–

The model is calibrated with respect to three different typologies of measure: performance, water transport and methanol cross-over.

The residuals between model results and experimental data have reasonably normal distribution and they are generally lower than measurement uncertainty for all the three typologies of measure. This implies that the model is sufficiently accurate to estimate the available experimental results and that the phenomena neglected with the proposed assumptions have minor effects. A comparison between simulated results and experimental measurements of water transport in two very different operating conditions is reported as example in Fig. 7.

All the obtained values of fitting parameters are coherent with those reported in literature. The fitting parameters of performance, Table 3, are composed of quantities affected by high uncertainty, demonstrated by a high variability in the literature [30,56–58]. The effective methanol diffusivity in the gas phase through the diffusion layer is noticeably uncertain, considering the contribution of CO_2 convective transport, the variation in void fraction and the methanol mixture phase transition. The obtained value is very close to that reported in Ref. [59]. The order of the overall anode reaction, γ^a, in literature varies from 0 [56] to 0.5 [30] to 1 [60]; the value obtained by calibration, 0.065, evidences a very weak current dependence on methanol concentration. With regard to the fitting parameters for flooding effects, the value of B_1 is very similar to that reported in Ref. [43], instead for the values of B_2 and B_3 there is no reference for comparison. Nevertheless the reduction of cathode diffusivity due to liquid water flux through cathode GDL can be considered reasonable and is discussed in the next section.

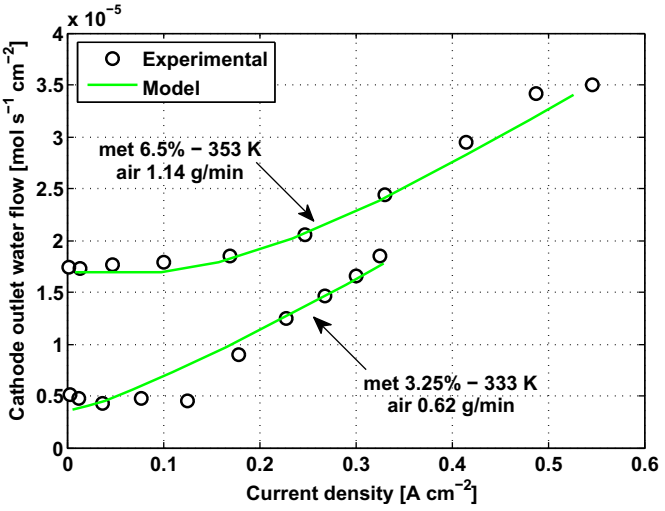

Fig. 7. Comparison of the simulated and measured water fluxes at cathode outlet (MEA GM, 1 bar).

The fitting parameters for water transport are reported in Table 4. For the fitting parameter W_2 there is no reference in literature; anyway the resulting values of $C^{m,c,L}_{H_2O}$, in the investigated conditions, are always coherent with a highly hydrated membrane. Electro-osmotic drag coefficient has a considerable variability [52]: most of the works reports a value of about 3 at 333 K [12,19,54], some studies higher values, near 6 [52,63], moreover this value can increase considerably when methanol is present [63]. The resulting value of 4.6 at 333 K is thus considered acceptable.

The fitting parameters reported in Table 5 characterize methanol cross-over through the membrane. C_3 is methanol drag coefficient, the fitting value, 1.82, lower than water drag coefficient, confirms the influence of methanol concentration gradient in the membrane, as reported in Ref. [38]. The dependence of electro-osmotic drag on temperature, C_4, is lower than that reported in Ref. [37], evidencing a limited effect of temperature.

Summarizing, the values of the parameters obtained by calibration result are acceptable and coherent with those reported in literature. This consideration, together with the high accuracy of the model in reproducing the experimental results, provides a first validation of the proposed interpretation and model of water transport in DMFC.

4.4. Modeling results discussion

Fig. 8a illustrates the water fluxes through the GDL at different current densities: when liquid permeation occurs, the magnitude of diffusion flux diminishes due to the increased water concentration in the cathode channel. At high current densities, when cathode flooding occurs, the permeation is the predominant water transport mechanism.

Table 3
Fitting parameters of performance.

		Present work	Literature
I_1	$cm^2\ s^{-1}$	2.17×10^{-2}	2.36×10^{-2} [59]
I_2	–	6.5×10^{-2}	0 [56], 0.5 [30], 1 [60]
I_3	–	0.5	0.5 [36]
I_4	$A\ cm^{-2}$	2.69×10^{-4}	94.25×10^{-4} [56] to 2×10^{-4} [36]
I_5	$J\ mol^{-1}$	66,712	70,000 [61]
B_1	–	37	[43]
B_2	–	5.24×10^2	–
B_3	–	0.8	–

Table 4
Fitting parameters of water transport.

		Present work	Literature
W_1	m^2	3×10^{-19}	2×10^{-18} [36] to 1×10^{-21} [56]
W_2	–	7.7×10^{-6}	–
W_3	$cm^2\ s^{-1}$	2.38×10^{-2}	1.55×10^{-2} [62]
W_4	–	4.6	2.9 [54] to 6 [63]

Fig. 8b reports the water fluxes through the membrane. It is interesting to note that permeation flux is negligible and is directed from cathode to anode. On the contrary the diffusion flux is always directed from anode to cathode; at low current densities it is the predominant water transport mechanism, due to a low water concentration at cathode side, while at high current densities it becomes negligible. The resulting trend of membrane water fluxes is coherent with that reported in Ref. [36].

In this paragraph a specific analysis of flooding effects on performance and a further validation of the model on MEA GG experimental results are reported.

4.4.1. Flooding effects

The developed model appears able to predict the flooding onset and to quantify its effects. Fig. 9 reports a comparison between simulation results with and without the implementation of flooding effects, in the same operating conditions of Fig. 7. At lower methanol concentration, the water flow at cathode outlet is low and the modeling results with and without the implementation of flooding effects are superimposed: this indicates that flooding does not occur. Instead at higher methanol concentration, where flooding is expected as discussed in Section 3.1, a considerable difference omitting flooding model is evident at high current density: this indicates that flooding occurs significantly at current densities higher than 0.4 A cm^{-2}.

A specific analysis is carried out to evaluate the contributions of the two flooding phenomena considered in the present model, superficial and bulk pore obstructions. Fig. 10 illustrates a comparison of modeling results excluding superficial or bulk pore obstruction correlations, in three different operating conditions, in order to distinguish and quantify their effects:

- in Fig. 10a, the effect of bulk obstruction is much more relevant than the superficial one;
- in Fig. 10b, water concentration in cathode channel increases due to the lower airflow rate, enhancing water condensation and superficial obstruction, nevertheless bulk obstruction is still more influent;
- in Fig. 10c, the saturation concentration diminishes due to the lower temperature, leading to a further enhancement of water condensation on GDL surface. In this case bulk and superficial obstructions are comparable.

Generally the effect of bulk obstruction is more relevant compared to the superficial obstruction one. However both types of obstruction must be taken into account to accurately reproduce experimental data: calibrating the model without one type of obstruction, the model accuracy decreases dramatically.

Fig. 11 reports the current density profiles along the channel at different voltages. From Fig. 9 it is possible to figure out that

Table 5
Fitting parameters of methanol crossover.

		Present work	Literature
C_1	$cm^2\ s^{-1}$	2.17×10^{-6}	0.5×10^{-6} [23] to 4.9×10^{-6} [36]
C_2	K	1976	2436 [36]
C_3	–	1.81	2.9 [37] to 0.87 [38]
C_4	K	410	1029 [37]

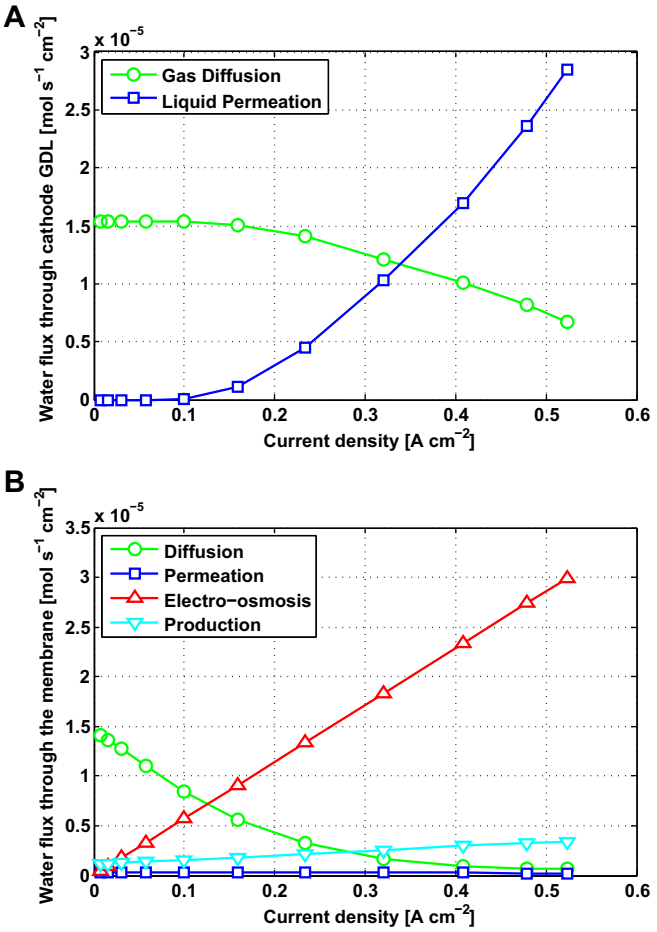

Fig. 8. Water fluxes through a) cathode GDL and b) membrane (MEA GM, met 6.5%, 353 K, air 1.14 g min^{-1}, 1 bar).

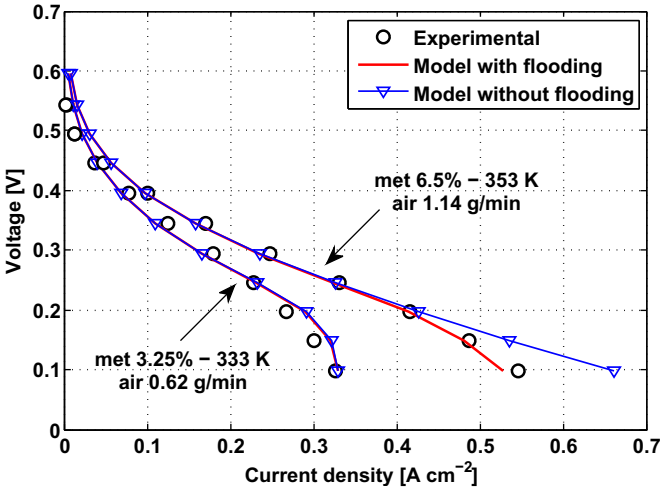

Fig. 9. Comparison of simulated performances with and without flooding effects (MEA GM, 1 bar).

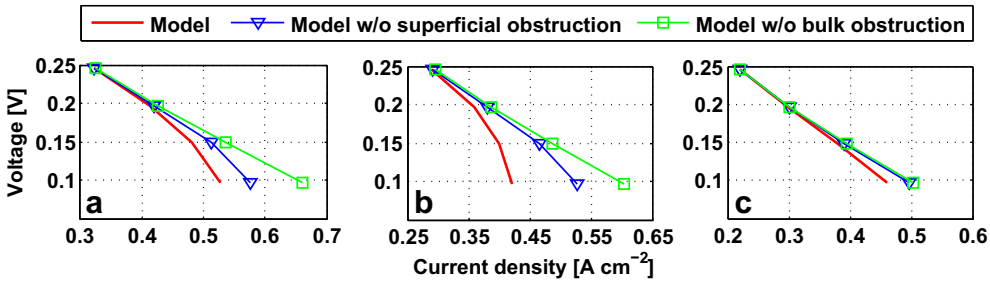

Fig. 10. Effects of superficial and bulk obstruction (MEA GM, 1 bar) a) met 6.5%, 353 K, air 1.14 g min^{-1}, b) met 6.5%, 353 K, air 0.62 g min^{-1}, c) met 6.5%, 333 K, air 0.62 g min^{-1}.

flooding occurs at voltages lower than 0.2 V. Analyzing the current density profiles, a flooding effect is already evident at 0.2 V: the current density profile presents a more steep decrease than at 0.3 V. The slope decreases even more at 0.1 V, evidencing a hindered fuel cell operation near channel outlet, caused by low oxygen concentration at cathode electrode. Such high current density gradient not only worsens performance, but could also determine inhomogeneous and aggravated components degradation.

Fig. 12 illustrates the reduction of cathode GDL effective diffusivity[5] at different voltages. At 0.3 V the reduction is in the order of 20% and it is only due to liquid permeation, i.e. bulk pore obstruction. At 0.2 V the reduction is more pronounced, in agreement with the higher water production and the steeper current density profile, Fig. 11. In this operating condition the water concentration in the channel reaches the saturation value approximately at two-thirds of the channel and consequently the effective diffusivity presents a further reduction due to superficial pores obstruction. At 0.1 V the superficial pores obstruction occurs nearly in the middle of the channel and the overall diffusivity at channel end is reduced by one order of magnitude: in this condition the cathode GDL is severely flooded.

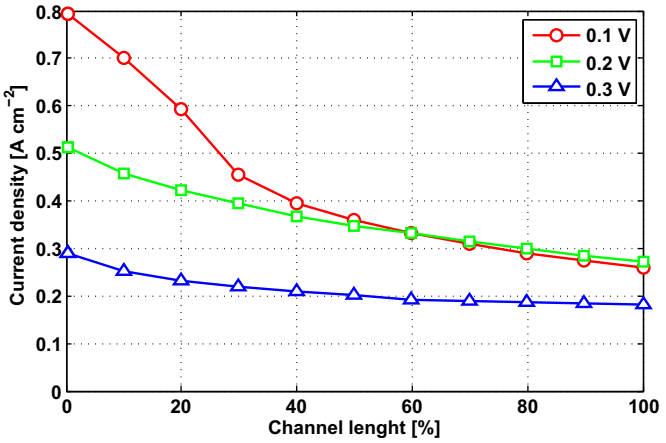

Fig. 11. Current density profiles at different voltages (MEA GM, met 6.5%, 353 K, air 1.14 g min^{-1}, 1 bar).

4.4.2. Cathode MPL influence

The model is further validated on the experimental data of the MEA GG (66 measurement points, three types of measures), Table 1. Two parameters, affected by the absence of cathode MPL, are calibrated. The parameters reported in Tables 2–5 remain valid, with the exception of the five parameters, related to cathode GDL, reported in Table 6.

It is interesting to note that the fitting parameter B_2, that quantify the bulk obstruction effect, is higher than the MEA GM one, Table 3: the bulk obstruction effect appears more relevant without cathode MPL at constant water permeation.

The fitting parameter W_2, that characterizes the dependence of $C^{m,c,L}_{H_2O}$ on capillary pressure, is higher compared to MEA GM one, Table 4: the lower GDL hydrophobicity implies a lower capillary pressure at constant membrane water concentration [17]. The p_{lim} value is assumed lower according to a less hydrophobic GDL compared to MEA GM one [55].

Although the uncertainty of material characteristics and the unpredictable interactions among components, the model is able to reproduce accurately the experimental data of MEA GG, Fig. 13. Moreover the model residuals are close to measurement uncertainty and the fitting parameters assume reasonable values. This result provides a further validation of both water transport and flooding proposed models.

The analysis of modeling results permits also to evaluate the cathode MPL influence. Fig. 13 points out the effect of flooding in two considerably different operating conditions. The behavior is similar to that reported in Fig. 9. At higher methanol concentration, two differences are appreciable: flooding effect magnitude increases and flooding onset occurs at lower current densities, nearly at 0.35 A cm^{-2}. These aspects are coherent respectively with the increase of bulk obstruction effect, B_2, and the reduction of breakthrough pressure, p_{lim}. This analysis confirms the explanation suggested discussing Fig. 4: the presence of cathode MPL increases mass transport resistance, reduces considerably water loss toward cathode channel and increases DMFC performance exclusively in case of significant GDL flooding.

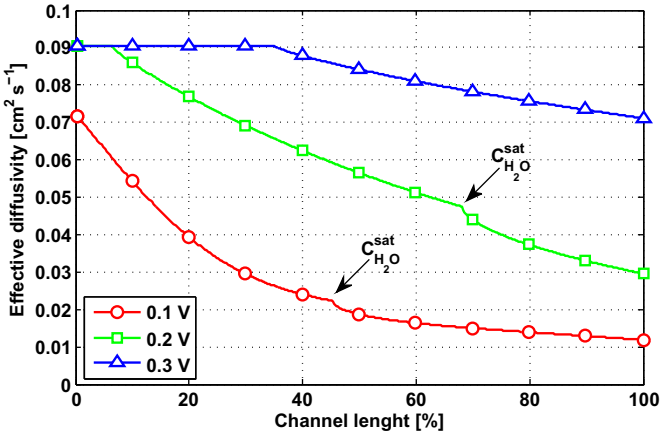

Fig. 12. Cathode GDL + MPL effective diffusivity profiles at different voltages (MEA GM, met 6.5%, 353 K, air 1.14 g min^{-1}, 1 bar).

[5] The GDL + MPL effective diffusivity is calculated with Formula (16) [43].

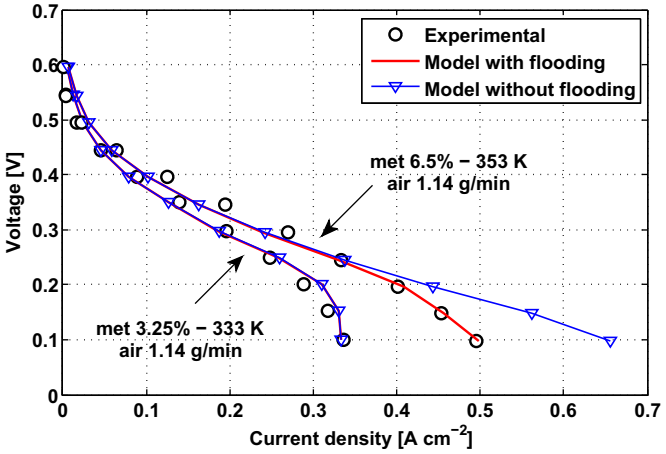

Fig. 13. Comparison of simulated performances with and without flooding effects (MEA GG, 1 bar).

Table 6
Fitted and assumed parameters for model validation (MEA GG).

B_2	–	6.21×10^2
W_2	–	2.76×10^{-5}
l^c_{MPL}	cm	0
l^c_{GDL}	cm	0.03
$p_{lim,GDL}$	Pa	1700 [55]

5. Conclusions

Water transport and flooding in DMFC are investigated through both experimental and modeling analyses. An exhaustive interpretation of the mechanisms that regulate these phenomena is proposed. The implemented model is able to reproduce accurately the experimental data. Such model is validated by means of three sets of experimental data (polarization curve, methanol crossover, water flow at cathode outlet), in an extensive range of operating conditions. The model includes also two correlations to reproduce the effects of cathode GDL flooding. A further validation of the model is carried out on the experimental data regarding a second DMFC with a different cathode GDL.

The modeling analysis permits also to examine both onset and magnitude of cathode GDL flooding and the influence of the MPL presence. The main conclusions on water transport and flooding phenomena are the followings:

- water transport through cathode GDL is regulated by two mechanisms: vapor diffusion and liquid water permeation; analyzing water flow at cathode outlet, the first determines a plateau at low current density; the second a linear trend at high current density; influence of temperature, pressure and airflow confirm the expectations;
- water diffusion through cathode GDL is regulated by vapor concentration gradient; in most of the investigated conditions vapor concentration in the electrode is close to saturation value, in agreement with a highly hydrated membrane;
- liquid water permeation through cathode GDL occurs when water pressure exceeds a threshold value, related to GDL characteristics; the permeation linear trend with current density is due to electro-osmotic drag and water production at cathode electrode;
- liquid water permeation through the membrane is directed from cathode to anode, while liquid water diffusion has the opposite direction with generally higher values; at low current densities diffusion is the predominant water transport mechanism;
- to reproduce the effects of cathode GDL flooding, two mechanisms have to be considered simultaneously, giving comparable contributions: superficial and bulk pore obstructions; the first is proportional to liquid water concentration in cathode channel; the latter is proportional to liquid water permeation;
- a correlation to reproduce bulk pore obstruction is proposed for two GDLs, with and without MPL; the magnitude of bulk obstruction effect is more relevant without cathode MPL;
- the addition of the MPL on cathode GDL increases the mass transfer resistance, causing a general reduction of water transport through cathode GDL; the performance decreases due to lower oxygen concentration when no flooding occurs, while performance increases with severe flooding, because the MPL limits its effect.

Acknowledgment

This work has been performed in the frame of the FCH FP7 project Premium Act (EC Grant Agreement 256776).

List of symbols

C	species concentration in channel (mol cm^{-3})
$\overline{C}$	time-average concentration in channel (mol cm^{-3})
C_{ref}	reference concentration (mol cm^{-3})
D_{eff}	effective diffusivity in diffusion layer (cm^2 s^{-1})
D_m	effective diffusivity in membrane (cm^2 s^{-1})
h_{conv}	convective mass transport coefficient (cm s^{-1})
E_0	ideal potential difference (V)
F	Faraday constant (C mol^{-1})
h	channel height and width (cm)
i	local current density (A cm^{-2})
i^*	exchange current density (A cm^{-2})
k	Tafel constant (A cm^{-2})
K_H	Henry constant (mol J)
L	channel length (cm)
l_m	membrane thickness (cm)
l	diffusion layer thickness (cm)
M	molecular weight (g mol^{-1})
m	inlet mass flow rate (g min^{-1})
K_m	membrane permeability (m^2)
N^{H2O}	water flux (mol cm^{-2} s^{-1})
X	molar or mass fraction (% or wt%)
N	flux (mol cm^{-2} s^{-1})
n_d	water drag coefficient
n_{dx}	methanol drag coefficient
p	channel pressure (Pa)
p_{sat}	saturation pressure (MPa)
p_{lim}	threshold breakthrough pressure (Pa)
R	universal gas constant (J mol^{-1} K^{-1})
R^G	mass transport coefficient in gas-phase (s cm^{-1})
T	fuel cell temperature (K)
v	local velocity in channel (cm s^{-1})
x	x coordinate (cm)

Greek symbol

α	Tafel transport coefficient
γ	reaction order
ε	volumetric void fraction
η	polarization (V)
σ_m	membrane conductibility (Ω^{-1} cm^{-1})
ρ	compound density (g cm^{-3})

μ	compound viscosity (Pa s)

Superscript

a	relative to anode
c	relative to cathode
t	relative to catalyst layer
G	relative to gas phase
L	relative to liquid phase
sat	relative to saturation

Subscript

GDL	relative to gas diffusion layer
MPL	relative to micro porous layer
m	relative to membrane
CO_2	relative to carbon dioxide
H_2O	relative to water
CH_3OH	relative to methanol
N_2	relative to nitrogen
O_2	relative to oxygen
air	relative to air
in	relative to channel inlet
out	relative to channel outlet
drag	relative to electro-osmotic drag
diff	relative to diffusion
cross	relative to cross-over
perm	relative to permeation
ox	relative to oxidation
rd	relative to reduction
tot	relative to total
conv	relative to convective

References

[1] J. Larmine, A. Dicks, Fuel Cell Systems Explained, second ed. Wiley, Chichester, West Sussex, 2003.
[2] C. Xu, T.S. Zhao, Electrochem. Commun. 9 (2007) 497–503.
[3] H. Yang, T.S. Zhao, Q. Ye, J. Power Sources 139 (2005) 79–90.
[4] C. Xu, T.S. Zhao, Q. Ye, Electrochim. Acta 51 (2006) 5524–5531.
[5] S.S. Sandhu, R.O. Crowther, J.P. Fellner, Electrochim. Acta 50 (2005) 3985–3991.
[6] F.Q. Liu, C.Y. Wang, Electrochim. Acta 53 (2008) 5517–5522.
[7] C. Xu, Y.L. He, T.S. Zhao, R. Chen, Q. Ye, J. Electrochem. Soc. 153 (2006) A1358–A1364.
[8] S. Kang, S.J. Lee, H. Chang, J. Electrochem. Soc. 154 (2007) B1179–B1185.
[9] M. Möst, M. Rzepka, U. Stimming, J. Power Sources 191 (2009) 456–464.
[10] E. Peled, A. Blum, A. Aharon, M. Philosoph, Y. Lavi, Electrochem. Solid State Lett. 6 (2003) A268–A271.
[11] A. Blum, T. Duvdevani, M. Philosoph, N. Rudoy, E. Peled, J. Power Sources 117 (2003) 22–25.
[12] X. Ren, W. Henderson, S. Gottesfeld, J. Electrochem. Soc. 144 (1997) L267–L270.
[13] G.Q. Lu, C.Y. Wang, J. Power Sources 134 (2004) 33–40.
[14] G.Q. Lu, F.Q. Liu, C.Y. Wang, Electrochem. Solid State Lett. 8 (2005) A1–A4.
[15] H. Kim, J. Oh, J. Kim, H. Chang, J. Power Sources 162 (2006) 497–501.
[16] F.Q. Liu, G.Q. Lu, C.Y. Wang, J. Electrochem. Soc. 153 (2006) A543–A553.
[17] C. Xu, T.S. Zhao, J. Power Sources 168 (2007) 143–153.
[18] T. Mennola, M. Noponen, T. Kallio, M. Mikkola, T. Hottinen, J. Appl. Electrochem. 34 (2004) 31–36.
[19] S. Ge, B. Yi, P. Ming, J. Electrochem. Soc. 153 (2006) A1443–A1450.
[20] B.S. Pivovar, Polymer 47 (2006) 4194–4202.
[21] J. St-Pierre, J. Electrochem. Soc. 154 (2007) B88–B95.
[22] G. Lin, T.V. Nguyen, J. Electrochem. Soc. 152 (2005) A1942–A1948.
[23] T. Schultz, K. Sundmacher, J. Membr. Sci. 276 (2006) 272–285.
[24] S.U. Jeong, E.A. Cho, H.J. Kim, T.H. Lim, I.H. Oh, S.H. Kim, J. Power Sources 159 (2006) 1089–1094.
[25] Q. Yan, H. Toghiani, J. Wu, J. Power Sources 158 (2006) 316–325.
[26] Q.X. Wu, T.S. Zhao, W.W. Yang, Int. J. Heat Mass Transfer 54 (2011) 1132–1143.
[27] W.W. Yang, T.S. Zhao, R. Chen, C. Xu, J. Power Sources 190 (2009) 216–222.
[28] C. Xu, T.S. Zhao, Y.L. He, J. Power Sources 171 (2007) 268–274.
[29] Y. Tian, G. Sun, Q. Mao, S. Wang, H. Liu, Q. Xin, J. Power Sources 185 (2008) 1015–1021.
[30] A.A. Kulikovsky, Electrochem. Commun. 7 (2005) 237–243.
[31] A.A. Kulikovsky, J. Appl. Electrochem. 30 (2000) 1005–1014.
[32] J. Divisek, J. Fuhrmann, K. Gaertner, R. Jung, J. Electrochem. Soc. 150 (2003) A811–A825.
[33] T. Schultz, K. Sundmacher, J. Power Sources 145 (2005) 435–462.
[34] J. Ko, P. Chippar, H. Ju, Energy 35 (2010) 2149–2159.
[35] W.W. Yang, T.S. Zhao, Electrochim. Acta 52 (2007) 6125–6140.
[36] C. Xu, T.S. Zhao, W.W. Yang, J. Power Sources 178 (2008) 291–308.
[37] A. Casalegno, R. Marchesi, D. Parenti, Fuel Cells 8 (2008) 37–44.
[38] A. Casalegno, R. Marchesi, J. Power Sources 185 (2008) 318–330.
[39] A. Casalegno, R. Marchesi, J. Power Sources 175 (2008) 372–382.
[40] U. Pasaogullari, C.Y. Wang, Electrochim. Acta 49 (2004) 4359–4369.
[41] A. Casalegno, C. Santoro, F. Rinaldi, R. Marchesi, J. Power Sources 196 (2011) 2669–2675.
[42] Env 13005, BIPM, IEC, IFCC, ISO, IUPAC, IUPAP, OIML, International Organization for Standardization, 1993, 1999, ISBN 92-67-10188-9.
[43] A. Casalegno, F. Bresciani, G. Groppi, R. Marchesi, J. Power Sources 196 (2011) 10632–10639.
[44] T.S. Zhao, C. Xu, R. Chen, W.W. Yang, Prog. Energy Combust. 35 (2009) 275–292.
[45] H. Li, Y. Tang, Z. Wang, et al., J. Power Sources 178 (2008) 103–117.
[46] S. Litster, D. Sinton, N. Djilali, J. Power Sources 154 (2006) 95–105.
[47] W.P. Liu, C.Y. Wang, J. Power Sources 164 (2007) 189–195.
[48] M.H. Shi, J. Wang, Y.P. Chen, J. Power Sources 166 (2007) 303–309.
[49] U. Pasaogullari, C.Y. Wang, J. Electrochem. Soc. 151 (2004) A399–A406.
[50] X. Ren, T.E. Springer, S. Gottesfeld, J. Electrochem. Soc. 147 (2000) 92–98.
[51] A. Oedegaard, C. Hentschel, J. Power Sources 158 (2006) 177–187.
[52] F. Meier, G. Eigenberger, Electrochim. Acta 49 (2003) 1731–1742.
[53] K. Jiao, X. Li, Prog. Energy Combust. 37 (2011) 221–291.
[54] T.A. Zawodzinski, C. Derouin, S. Radzinski, R.J. Sherman, V.T. Smith, T.E. Springer, S. Gottesfeld, J. Electrochem. Soc. 140 (1993) 1041–1047.
[55] Z. Lu, M.M. Daino, C. Rath, S.G. Kandlikar, Int. J. Hydrogen Energy 35 (2010) 4222–4233.
[56] Z.H. Wang, C.Y. Wang, J. Electrochem. Soc. 150 (2003) A508–A519.
[57] K. Scott, W. Taama, J. Cruickshank, J. Power Sources 65 (1997) 159–171.
[58] H. Guo, C. Ma, Electrochem. Commun. 6 (2004) 306–312.
[59] A.A. Kulivkovsky, J. Divisek, A.A. Kornyshev, J. Electrochem. Soc. 147 (2000) 953–959.
[60] J. Ge, H. Liu, J. Power Sources 160 (2006) 413–421.
[61] S.Lj. Gojkovic, T.R. Vidakovic, D.R. Durovic, Electrochim. Acta 48 (2003) 3607–3614.
[62] R.H. Perry, D.W. Green, Perry's Chemical Engineer's Handbook, McGraw-Hill, 1999.
[63] T. Tschinder, T. Schaffer, S.D. Fraser, V. Hacker, J. Appl. Electrochem. 37 (2007) 711–716.
[64] NIST Standard Reference Database 106, IUPAC-NIST Solubility Database, 2003.